

PEDESTRIAN KINEMATICS INVESTIGATION WITH FINITE ELEMENT DUMMY MODELS BASED ON ANTHROPOMETRY SCALING METHOD

Costin Untaroiu

Jaeho Shin

Johan Ivarsson

Jeff Crandall

Center of Applied Biomechanics, University of Virginia,
United States

Yukou Takahashi

Akihiko Akiyama

Yuji Kikuchi

Honda R&D Co., Ltd.

Japan

Paper Number 07-0328

ABSTRACT

Pedestrian-vehicle impact experiments using cadavers have shown that factors such as vehicle shape and pedestrian anthropometry can influence pedestrian kinematics and injury mechanisms. While a parametric study examining these factors could elucidate the complex relationships that govern pedestrian kinematics, it would be impractical with cadaver tests due to the relative expense involved in performing numerous experiments on subjects with varying anthropometry. On the other hand, finite element (FE) modeling represents a more feasible approach since numerous experiments can be conducted for a fraction of the expense. The current study examined the relationship between pedestrian anthropometry and front shape of a mid-size sedan using a PAM-CRASH model of the 50th percentile male (50th) Polar-II pedestrian dummy extensively validated against experimental data. In order to evaluate the influence of pedestrian anthropometry on response kinematics, scaled dummy models were developed based on the weight and height of the 5th percentile female (5th F) and 95th percentile male (95th M). Simulations of the 5th F, 50th F, 50th M, and 95th Polar-II FE models struck at 40 km/h by a mid-size sedan were used to generate trajectories of the head, upper thorax, mid-thorax, and pelvis. In an effort to assess the validity of scaling techniques when interpreting trajectory data from vehicle-pedestrian crashes, the trajectories of the 5th F, 50th F and 95th M model were scaled to the 50th M and compared to those generated with the 50th model. The results demonstrated nonlinear behavior of dummy kinematics that could not be accounted for with traditional linear scaling techniques.

INTRODUCTION

The pedestrian is one of the most vulnerable road users and comprise about 65 percent of the 1.17 million annual traffic related fatalities in the world (World Bank, 2007). The probability for a pedestrian to be injured or killed is much higher than that for a vehicle occupant. In 2005, 8.7% of vehicle-pedestrian impacts in the US were fatal, whereas the corresponding fatality rate for occupants in crashes only was 1.3% (NHTSA, 2007).

Protection of pedestrians in car-to-pedestrian collisions (CPC) has recently generated increased attention with regulations implemented or proposed in Europe (EEVC, 2002), Korea (Youn et al., 2005), and Japan. While subsystem experiments are currently being used as the basis of evaluations for these regulations, car-to-pedestrian dummy impact tests or car-to-human/dummy impact simulations provide complimentary data that better describe the complete vehicle-pedestrian interaction.

An advanced pedestrian dummy, called Polar-II, has been developed and continuously improved by Honda R&D, GESAC, and the Japan Automobile Research Institute (JARI) (Akiyama et al., 1999, 2001; Okamoto et al., 2001, Takahashi et al., 2005, Crandall et al., 2005). While the dummy incorporates advanced instrumentation in the head, neck, chest, pelvis, and lower limbs (Akiyama et al. 2001), the primary purpose of the Polar-II dummy was reproducing pedestrian kinematics in a collision with a vehicle. Kerrigan et al. (2005a, b) performed vehicle impact tests on the Polar-II and post mortem human surrogates (PMHS) in identical conditions and showed that the Polar-II dummy generally replicates the complex kinematics of the PMHS. However, the

Polar-II dummy has the general characteristics of the 50th percentile male and can therefore not predict kinematics for all statures of pedestrians.

A FE model of the Polar-II dummy has been developed, validated in component tests (Shin et al. 2006), and verified at the full scale level against kinematic data (Shin et al. 2006, 2007) recorded during the vehicle-dummy impact experiments performed by Kerrigan et al. (2005). The Polar-II FE model was developed using Hypermesh (Altair Engineering) and Generis (ESI) as pre-processors and PAM-CRASH/PAM-SAFE FE solver (version 2001, ESI) was used for impact simulations. The model contains 27,880 elements that represent the head, neck, thorax, abdomen, pelvis, upper arms, forearms, hands, thighs, knees, legs, and feet and has a total mass and height close to that of the 50th percentile male.

It is believed that pedestrian kinematics is highly influenced by vehicle geometry and pedestrian anthropometry (Mizuno, 2005). While the dependence of pedestrian kinematics on vehicle geometry has been previously shown (Kerrigan et al 2005 a, b), there have been few studies presenting the influence of the pedestrian adult anthropometry (Shin et al 2007). Thus vehicle-pedestrian simulations were performed with a mid-size sedan vehicle model and a family of dummies corresponding to peaks and extremes of the adult population (Figures 1 and 2), and the trajectories of several upper body locations were calculated. Additionally, a traditional height scaling technique of PMHS trajectories to those corresponding to the 50th percentile male has been evaluated using the kinematic response of scaled dummies.

METHODOLOGY

Pedestrian Anthropometric Data

The development of pedestrian dummies requires the anthropometric data of subjects in standing posture. Most anthropometric data have been gathered for subjects in a typical semi-reclined seated posture for design of occupant dummies (e.g. Schneider et al. 1985, Seidl 1997). A few studies (e.g. Gordon et al. 1998, Anthropometric Source Book 1978) also considered anthropometric characteristics of the standing posture. The Anthropometric Survey (ANSUR) of U.S. Army Personnel conducted during the two-year period from 1987 to 1988 (Gordon et al. 1989) includes over 132 anthropometric measurements collected for 9,000 subjects in standing and sitting postures. This database showed symmetric distributions of height and mass around average values, those considered to

correspond to the 50th percentile of anthropometric subjects (Figures 1 and 2). To study the influence of anthropometry on pedestrian kinematics in lateral car-to-pedestrian impacts, four dummy models were created:

- a 50th M and a 50th F which represent the adult population peaks
- a 5th F and a 95th M which represent extreme subjects of the adult population

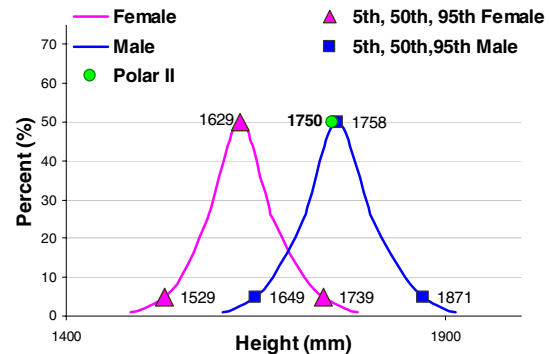


Figure 1: Height Distribution

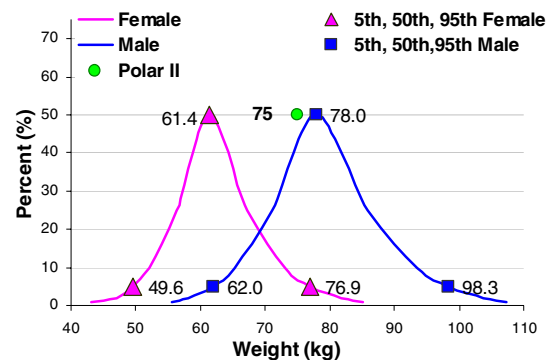


Figure 2: Weight Distribution

The Polar-II FE model (Shin et al 2006) was used to represent the 50th percentile male because it closely approximated the anthropometric characteristics (Figures 1 and 2). The other three models were derived by scaling this model according to the methodology presented in the next section.

Scaling of the Polar-II FE Model

Scaling of Dummy Geometry

A preliminary study of the ANSUR anthropometric data revealed non-proportional variations in all anatomical directions of body measurements for all anthropometric subjects under study (5th F, 50th F, 50th M, and 95th M) which make scaling a challenging task. For the purpose of the

current study, we selected mass and height as the most important anthropometric characteristics to match with the corresponding data of ANSUR subjects. Therefore, the scaling of each model was performed in two steps:

- scaling in vertical direction (z-axis) – to match the stature(height)

$$\lambda_{z,subject} = \frac{H_{subject}}{H_{Polar-II}} \quad (1)$$

- scaling in the transverse plane (x-y plane) – to match the total mass

$$\lambda_{x,subject} = \lambda_{y,subject} = \sqrt{\frac{m_{subject}}{m_{Polar-II} \lambda_{z,subject}}} \quad (2)$$

To verify the scaled dummy models obtained according to this methodology: 5th percentile female (5F-S), 50th percentile female (50F-S), and 95th percentile male (95M-S), several specific anthropometric dimensions of the scaled models and the Polar-II model were compared with the corresponding data of the ANSUR subjects. These specific dimensions in all anatomical directions (Figure 3) are: cervical height (1), iliocristale height (2), vertical thumbtip reach down (3), knee height (4), menton-top of head (5), head breadth (6), bideltoid breadth (7), waist breadth (8), chest depth (9), and buttock depth (10).

Scaling of Inertial Properties

The components of the Polar-II model can be classified as either deformable or rigid parts. Using the mass densities of each component, that was assumed constant between the Polar-II FE model and scaled dummy models, the inertial properties (mass and the components of the inertia tensor) of the deformable parts were calculated from their meshes. The inertial properties of rigid bodies, which usually have simplified meshes, were defined in the input file of the model based on measurement data. As a consequence, an algorithm for obtaining the mass and components of the inertia tensor relative to new centers of gravity of scaled rigid models was developed (see Appendix) and applied for all scaled dummy models. The same factors used to scale the dummy geometry were also used to scale inertia properties of rigid parts.

Scaling of Joint Properties

Several components of the dummy are connected by defined joint models for which the joint stiffness is characterized by a moment-angle curve. Based on the principles of dimensional analysis (Langhaar, 1951), the moment of a scaled entity can

be expressed as a function of the length scale factors (Ivarsson et al. 2004):

$$M_{scaled} = \lambda_x \lambda_y \lambda_z M_{Polar-II} \quad (3)$$

As a result, all moment-angle curves of the scaled dummy models were scaled using this equation.

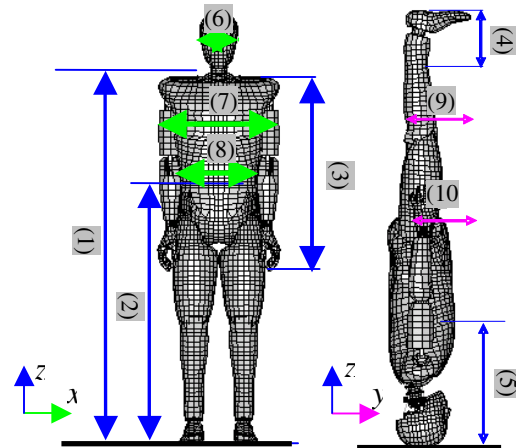


Figure 3: Anthropometric dimensions used to compare scaled dummy models with corresponding ANSUR data (Gordon et al. 1989)

Vehicle-Pedestrian Simulations

Four full-scale pedestrian impact simulations were performed using the Polar-II dummy model and scaled dummy models. The methodology used to perform these simulations was similar to that used in previous verification studies presented by Shin et al. (2006, 2007). The Polar-II dummy model was positioned laterally at the vehicle-centerline in a mid-stance gait with the left lower extremity in the leading position and the right lower extremity closest to the vehicle (a mid-size sedan). To promote repeatability and reduce test-to-test variability, the upper extremities were bound at the wrist with the left wrist closer to the abdomen. A plane simulating the ground level was specified and a pre-impact preload was applied just before impact through an initial feet-ground penetration corresponding to the dummy weight. The front-end of the vehicle model included all exterior structures that could contact the dummy as well as the stiff underlying structures (e.g., engine components) that could be loaded by the exterior vehicle structures during the impact. The mass of the simplified vehicle model was adjusted to the mass of the vehicle sled buck by adding the mass differential to the vehicle CG. A 40 km/h initial velocity in the impact direction (towards the pedestrian) was applied to the vehicle model at the beginning of the simulations. Kinematic trajectories of the head center of gravity (CG), T1

(i.e., top of thoracic spine), T8 (i.e., mid-thoracic spine) and pelvis CG (locations of the photo targets used in the full scale PMHS tests by Kerrigan et al., 2005 a, b) were calculated to allow for comparison with body segment trajectories of four different dummy models (Figure 4). Additionally, the wrap around distance (WAD) to head contact was calculated in all simulations.

To provide a basis for validation of the pedestrian dummy against the PMHS data, the PMHS kinematic response was linearly scaled to the 50th percentile male's response using a length scale factor. Thus, the original PMHS trajectories for $x(t)$ and $z(t)$ together with time were scaled using the height ratio of the PHMS relative to the 50th percentile male (Kerrigan et al. 2005 a, b). In order to verify the validity of this method, all trajectories of the dummy models (5F-S, 50F-S, and 95M-S) were scaled to Polar-II (50th percentile male model) data using the same methodology. The percentage error between scaled trajectories and the corresponding Polar-II trajectories were calculated according to (4).

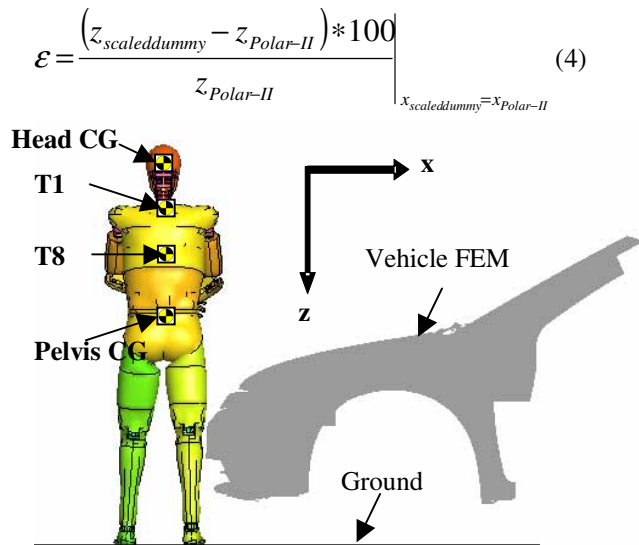


Figure 4: Node set of the pedestrian dummy model used in the kinematics analysis.

RESULTS

Polar-II Scaled Dummy Models

Three new dummy FE models -5F-S, 50F-S, and 95M-S (Figure 5)- were obtained by scaling the Polar-II model with the factors calculated using equations 1 and 2 and listed in Table 1. While the scaling of 5th and 50th percentile female dummy models involved almost uniform scaling (under 1 %

variation between λ_z and $\lambda_x=\lambda_y$ scaling factors), a substantial variation (3.4 %) was observed between scaling factors in the x-y plane and the z-direction of the 95th percentile male model.

The specific body measurements (Figure 3) of each dummy model exhibit good agreement with the corresponding data of the ANSUR subjects. Polar-II dimensions are similar ($\pm 2\%$) in all directions with the corresponding dimensions of the ANSUR 50th percentile male. While specific dimensions of the scaled dummy models in the z-direction (Figure 6) are close to corresponding values of the ANSUR subjects ($\pm 2\%$), several variations ($\pm 6\%$) in the x-y plane were recorded (Figure 7). All scaled dummy models have the same height and mass as their corresponding ANSUR subjects (5th female, 50th female and 95th male).

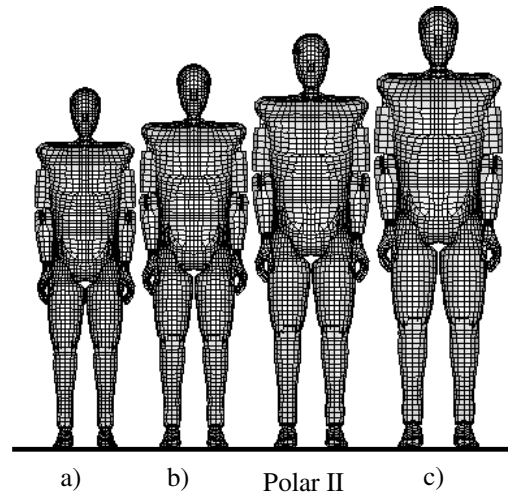


Figure 5: Polar II FE model and its scaled models: 5th female (5F-S) (a), 50th female (50F-S) (b), and 95th male (95M-S) (c).

Table 1. The factors used to obtain dummy FE models by scaling the Polar-II FE model (50th percentile male)

Dummy Model	Scale Factors	
	λ_z	$\lambda_x=\lambda_y$
5 th percentile female	0.873	0.871
50 th percentile female	0.93	0.938
95 th percentile male	1.069	1.107

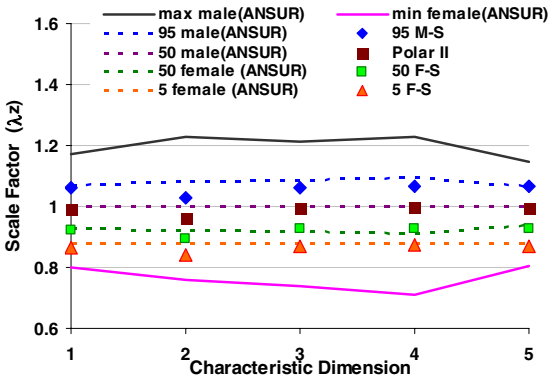


Figure 6: Specific dimensions (vertical direction) normalized to corresponding dimensions of the 50th percentile ANSUR male (Gordon et al. 1989). Comparison between Polar-II scaled models and ANSUR data

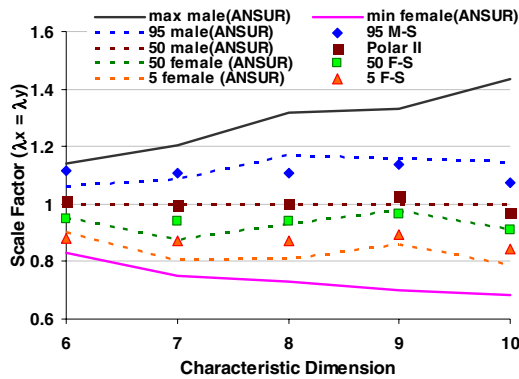


Figure 7: Specific dimensions (transversal plane) normalized to corresponding dimensions of the 50th percentile ANSUR male (Gordon et al. 1989). Comparison between Polar-II scaled models and ANSUR data

Vehicle-Dummy Lateral Impact Simulations

Dummy posture relative to the vehicle at the time of head impact for the original Polar-II (50th male) dummy and the scaled dummy models are illustrated in Figure 8. In all cases, the car-pedestrian dummy head impacts occurred in the windshield region, except for the 5th female dummy model for which the vehicle-head impact took place in the cowl region. The Polar-II 50th male WAD to head contact obtained from the simulation (1959 mm) was within the range of Polar-II experimental test data (1947 ±21 mm) suggesting good kinematic predictability of the FE dummy model (Figure 9). A linear variation of WAD to head contact with respect to dummy height was observed in both simulations using FE dummy models ($R^2=0.996$) and PMHS tests ($R^2=0.899$)

(Kerrigan et al. 2005a). However, the dummy WAD obtained from simulations and Polar-II test data (Kerrigan et al., 2005) were lower than that of the corresponding value of the PMHS data (Figure 9).

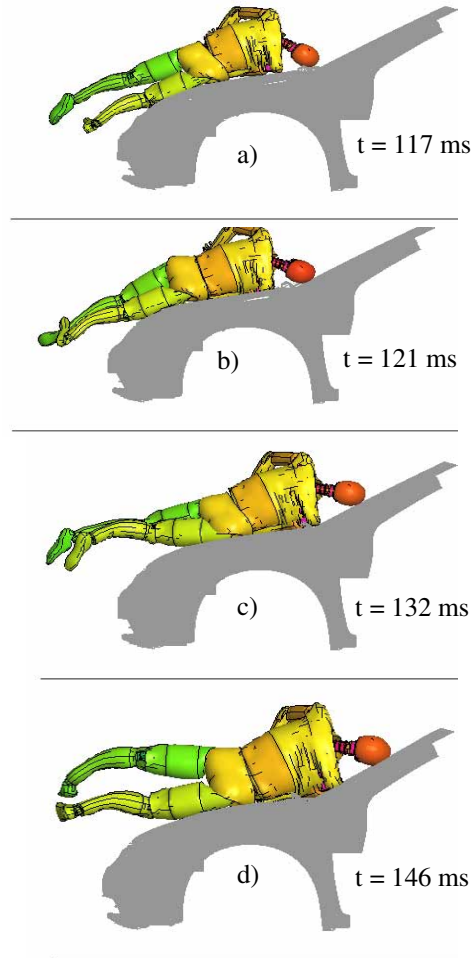


Figure 8: 5F-S (a), 50F-S (b) Polar-II (50th percentile male) (c), and 95M-S dummy models at the pedestrian head strike time.

Kinematic trajectories of the head CG, T1, T8 and pelvis CG together with their trajectory corridor (area bordered by the extreme trajectories) are illustrated in Figures 10, 11, 12, and 13. All trajectory curves were calculated until head strike in a system fixed with respect to the vehicle's motion, which was called the Vehicle Coordinate System (VCS). The origin of the VCS system is defined by the intersection of the vertical line (z-axis) passing through the initial position of the dummy head CG and the horizontal line (x-axis) of the ground level (Kerrigan et al. 2005). A linear variation of upper body trajectories are observed between the time the bumper strikes the legs and the time the dummy pelvis flesh starts to interact with the leading edge of

the hood. However, after that point, a strong non-linearity was observed in all pelvis CG trajectories. Kerrigan et al. (2007) have indicated that this may be a function of the pelvis sliding over, penetrating into, or bouncing off the hood depending on the extent of pelvic interaction with the leading edge of the vehicle. The largest pelvis bounce was observed in the 5F-S dummy model for which some of the upper body trajectories (pelvis CG, T1, and T8) were closer or even slightly higher than the corresponding trajectories of a taller dummy model – 50 F-S dummy.

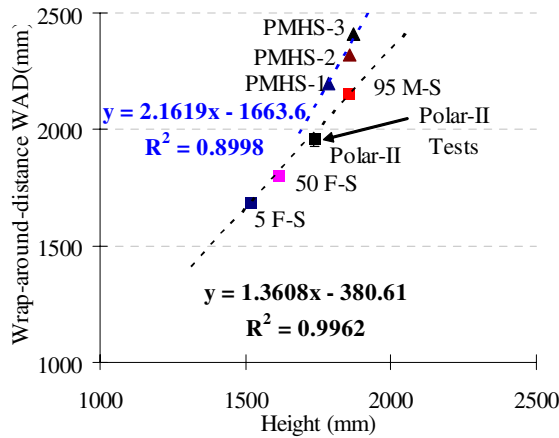


Figure 9: WAD to head contact vs. height curves. Comparison between Polar-II and dummy results and PMHS data (Kerrigan et al 2005a)

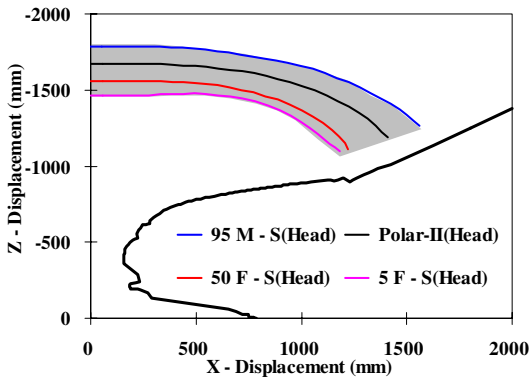


Figure 10: Head- Center of gravity (CG) trajectory corridor and comparisons between the Polar-II and scaled dummy models

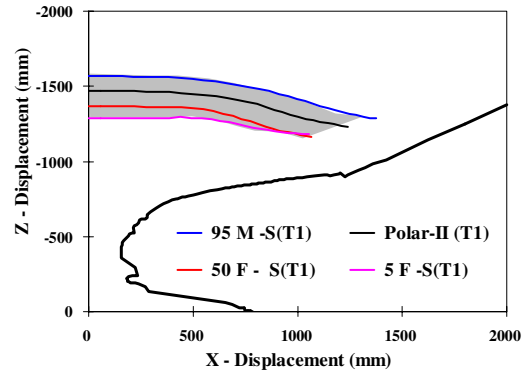


Figure 11: T1 trajectory corridor and comparisons between the Polar-II and scaled dummy models

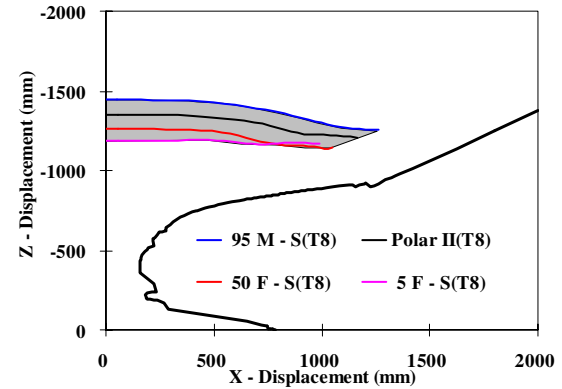


Figure 12: T8 trajectory corridor and comparisons between the Polar-II and scaled dummy models

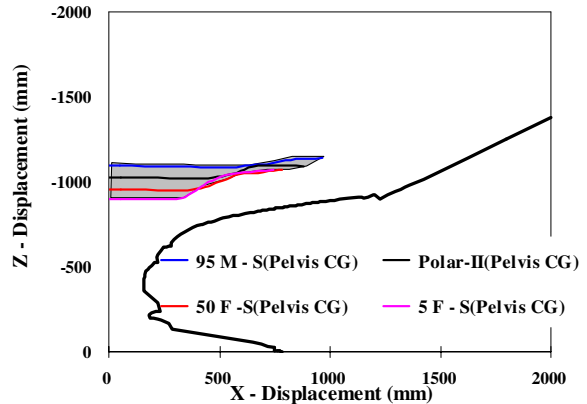


Figure 13: Pelvis CG trajectory corridor and comparisons between the Polar-II and scaled dummy models

Upper body trajectories of the 5 F-S, 50 F-S and 95 M-S scaled to the corresponding data of

Polar-II (50th percentile male) are illustrated in Figures 14 and 15. These scaled curves have two portions delimited by specific events: 1) after bumper-leg contact but before pelvis flesh-leading edge contact and 2) after pelvis flesh-leading edge contact but before head strike. As expected, in the first part, scaled trajectories matched very well the corresponding trajectories of the Polar-II (50th percentile male). However, significant differences between scaled trajectories and corresponding 50th percentile trajectories appear in the second region, especially close to the time of head strike. The maximum error between these trajectories calculated as the percentage difference between vertical displacements at the same horizontal level are illustrated in Figure 16. As can be observed, the scaled trajectories of the 5F – S dummy overestimate the corresponding Polar-II trajectories for all recorded upper body segments, with the error decreasing from pelvis to head region. A similar trend is also observed for scaled trajectories of the other dummy that is smaller than the Polar-II (50F-S). However, while the pelvis CG/T8 scaled trajectories overestimate the corresponding Polar-II (50th male) trajectories, T1/head CG scaled trajectories underestimate the corresponding Polar-II trajectories. In case of the largest dummy- 95M-S, the maximum error of upper body scaled trajectories shows an opposite trend. While the pelvis CG, T8, and T1 underestimate the corresponding 50th male trajectories, an overestimation is recorded in scaled trajectory of the head CG. Overall, the maximum error of all scaled trajectories varies from -12 % (50th female head CG) to +11.6% (5th female pelvis CG).

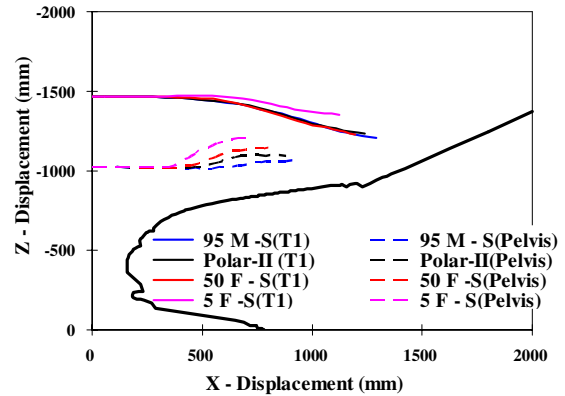


Figure 15: T1 and pelvis CG trajectory comparisons between the Polar-II and scaled dummy models

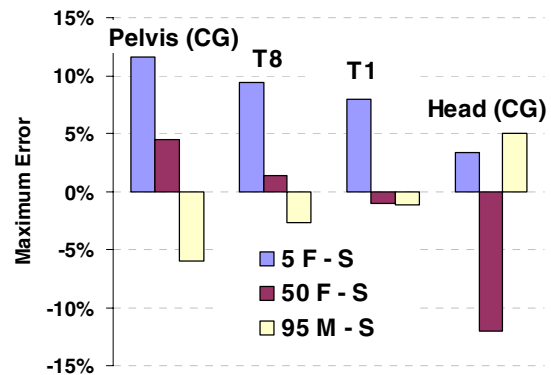


Figure 16. The maximum error (%) of the scaled pedestrian trajectories

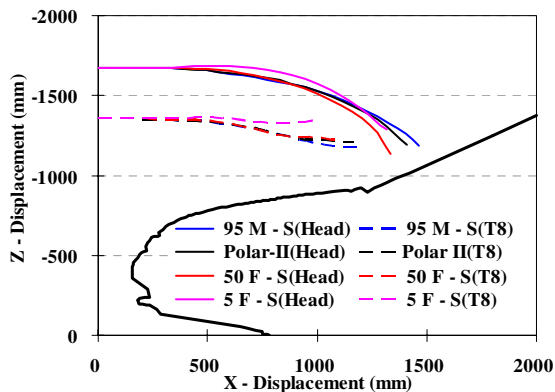


Figure 14: Scaled Head CG and T8 trajectory comparisons between the Polar-II and scaled dummy models

DISCUSSION

Three new FE pedestrian dummy models were obtained using the validated FE Polar-II dummy model as reference (Shin et al. 2006, 2007). Uniform scaling in the vertical direction and transverse plane was used to obtain FE dummy models corresponding to three representative ANSUR subjects (5th female, 50th female, and 95th male). While several differences between specific dimensions of scaled models and anthropometric data (maximum 7% in transversal plane) were observed, global dummy characteristics (height and mass), which may have a major role in pedestrian kinematics during a vehicle impact, were matched by this scaling technique. In addition, specific vertical dimensions of scaled dummies, which may have a significant influence on the vehicle-pedestrian interaction due to joint positions, showed minor differences (under 2%)

relative to anthropometric data. The scaling method used in the current study to obtain new dummy models with different anthropometry from a reference model shows easy implementation and relatively good results. While differences between all specific dimensions of dummy and anthropometric data may be reduced by using more complex scaling techniques (c.f., Kriging method used for scaling a pelvis FE model by Besnault et al., 1998) with specific scaling factors for each body segments, the effort to connect scaled body parts into the whole dummy scaled model will increase considerably. Due to lack of test data between joint properties and anthropometry, joint stiffness properties of the new dummy models were obtained by scaling Polar-II stiffness curves (Langhaar, 1951). Therefore, when this data will be available in literature, an update of joint stiffness curves for all scaled models is recommended.

A complex variation of pedestrian upper body trajectories was observed in simulations of vehicle-pedestrian lateral impacts with different sized dummies and the same vehicle model having a 40km/h initial velocity. Dummy trajectory corridors, defined as the surface which covers all dummy trajectories, are uniform during the initial phase of impact but demonstrate different behavior after pelvic interaction with the hood leading edge and before head strike. While the pelvis CG corridor narrows after the pelvis flesh starts to interact with leading edge, a significant extension of the head CG corridor is recorded for the same period. Trajectory corridors with almost constant widths are recorded for T1 and T8 trajectory corridors before head strike event

In dummy simulations as in PMHS tests (Kerrigan et al. 2005) linear relationships were observed between WAD and pedestrian height. However, the dummy models predict lower WADs than the PMHS tests. A potential cause of these kinematic differences between dummies and PMHSs could be the musculature effects in the neck, spine and chest which have been incorporated in the dummy models (Crandall et al., 2005).

Linear scaling of dummy upper body trajectories to the corresponding responses of the 50th male with respect to dummy height showed important limitations. A consistent error pattern in terms of vertical displacement for a certain horizontal displacement was identified between the scaled dummy trajectories based on dummy size and the location of recorded targets. The scaled trajectories of smaller dummies tended to overestimate the corresponding response of the 50th male model in regions close to pelvis and to underestimate (or in the case of the 5th female, to overestimate) the regions

close to the head. The opposite pattern was observed for the taller dummy model (95th male). While the current study is limited to only one vehicle type, one vehicle speed, and one pedestrian orientation, these observations suggest that the linear scaling of upper body trajectories must be used cautiously with an awareness of the inherent assumptions and limitations. Ultimately, the results suggest that an advanced non-linear approach must be developed to predict the correct kinematics. Alternatively, a complete family of physical and/or computational dummy models will be required to describe the complexity of the pedestrian-vehicle interaction as a function of their relative geometry.

CONCLUSIONS

Three finite element dummy models of different anthropometry were obtained by scaling the Polar-II dummy – a pedestrian dummy previously validated in pedestrian impact conditions. All dummy models, which were intended to represent the anthropometric breadth of the general adult population, have similar mass and height characteristics as equivalent subjects obtained from an anthropometric database. In addition to stature and mass, several specific body measurements also showed agreement with the corresponding anthropometric data. The dummy models were used to study the influence of pedestrian anthropometry on kinematic responses in vehicle-pedestrian impact simulations. While the WAD to head contact demonstrated a linear relationship with the dummy height, upper body trajectories appeared to be influenced by the target location and dummy size. Thus linear scaling of PMHS trajectories to the corresponding 50th percentile male trajectories has potentially significant limitations in terms of reproducing the correct kinematics.

REFERENCES

- [1] Akiyama A., Yoshida S., Matsushashi T., Moss S., Salloum M., Ishikawa H., Konosu A. (1999) Development of Human-like Pedestrian Dummy, Paper 9934546, Japanese Society of Automotive Engineers, Chiyoda-Ku, Tokyo, Japan.
- [2] Akiyama A., Okamoto M., N. Rangarajan (2001) Development and Application of the New Pedestrian Dummy, Paper 463, Proceedings of the 17th International Technical Conference on the Enhanced Safety of Vehicles (ESV), Amsterdam, The Netherlands.

[3] Besnault B., Guillemot H., Robin S., Lavaste F., Le Coz J.Y. (1998) A parametric finite element model of the human pelvis. 42nd Stapp Car Crash Conference. 1998.

[4] Crandall J., Wiley K., Longhitano D., Akiyama A. (2005) Development of Performance Specifications for a Pedestrian Research Dummy, Paper 05-0389, Proceedings of the 19th International Technical Conference on the Enhanced Safety of Vehicles (ESV), Washington DC, United States.

[5] European Enhanced Vehicle-Safety Committee, EEVC Working Group 17 Report—Improved Test Methods to Evaluate Pedestrian Protection Afforded by Passenger Cars, www.eevc.org, (December 1998 with September 2002 updates).

[6] Gordon, C.C., Churchill, T., Clauser, C.E., Bradtmiller, B., McConville, J.T., Tebbetts, I., Walker, R.A. (1989). 1988 Anthropometric Survey of U.S. Army Personnel: Methods and Summary Statistics. Final Report (NATICK/TR-89/027) U.S. Army Natick Research Development and Engineering Center, Natick, Massachusetts.

[7] Ivarsson B.J., Crandall J., Longhitano D., Okamoto M. (2004) Lateral Injury Criteria for the 6-year-old Pedestrian – Part I: Criteria for the Head, Thorax, Neck, Thotax, Abdomen and Pelvis, Paper 2004-01-0323, Society of Automotive Engineers.

[8] Kerrigan J., Murphy D., Drinkwater C., Kam C. Y., Bose D., Crandall J. (2005a) Kinematic Corridors for PMHS Tested in Full-Scale Pedestrian Impact Tests, Paper 05-0394, Proceedings of the 19th International Technical Conference on the Enhanced Safety of Vehicles (ESV), Washington DC, United States.

[9] Kerrigan J., Kam C., Drinkwater C., Murphy D., Bose D., Ivarsson J., Crandall J. (2005b) Kinematic Comparison of the Polar-II and PMHS in Pedestrian Impact Tests with a Sport-Utility Vehicle, Proceedings of the 2005 International Research Council on the Biomechanics of Impact (IRCOBI), Prague, Czech Republic.

[10] Kerrigan J., Crandall J., Deng B. (2007) Pedestrian Kinematic Response to Mid-sized Vehicle Impact, International Journal of Vehicle Safety, in press

[11] Langhaar, H. L. (1951) Dimensional Analysis and Theory of Models. John Wiley & Sons, Inc., New York.

[12] Mizuno Y. (2005) Summary of IHRA pedestrian Safety WG Activities (2005) – Proposed Test Methods to Evaluate Pedestrian Protection Affordable by Passenger Cars

[13] NASA. Anthropometric Sourcebook (1978). NASA Reference Publication No. 1024, Houston TX

[14] National Highway Traffic Safety Administration (NHTSA), (2007) <http://www-nrd.nhtsa.dot.gov/Pubs/overviewtsf05.pdf>

[15] Okamoto Y., Akiyama A., Okamoto M., Kikuchi Y. (2001) A Study of the Upper Leg Component Tests Compared with Pedestrian Dummy Tests, Paper 380, Proceedings of the 17th International Technical Conference on the Enhanced Safety of Vehicles (ESV), Amsterdam, The Netherlands.

[16] Pam System International, (2004) PAM-CRASH / PAM-SAFE REFERENCE MANUAL, Version 2004.

[17] Seidl, A., ‘RAMSIS – A New CAD Tool for Ergonomic Analysis of Vehicles Developed for the German Automotive Industry’. Tecmath GmbH, SAE Paper 970088.

[18] Schneider, L.W., Robbins, D.H., Pflüg, M.A., and Snyder, R.G., (1985) ‘Development of an Anthropometrically based Design Specifications for an Advanced Adult Anthropomorphic Dummy Family’. Volumes 1-3, Final Report DOT-HS-806-715. National Highway Traffic Safety Administration U.S. Department of Transportation, Washington D.C.

[19] Shin J., Lee S., Kerrigan J., Darvish K., Crandall J., Akiyama A., Takahashi Y., Okamoto M., Kikuchi Y. (2006) Development and Validation of a Finite Element Model for the Polar-II Upper Body, Paper 2006-01-0684, Society of Automotive Engineers.

[20] Shin J., Untaroiu C., Kerrigan J., Crandall J., Subit D., Takahashi Y., Akiyama A., Kikuchi Y., Longitano D. (2007) Investigating Pedestrian Kinematics with the Polar-II Finite Element Model, Paper 2007-01-0756 Society of Automotive Engineers.

[21] Takahashi Y., Kikuchi Y., Okamoto M., Akiyama A., Ivarsson J., Bose D., Subit D., Shin J., Crandall J. (2005) Biofidelity Evaluation for the Knee and Leg of the Polar Pedestrian Dummy, Paper 05-0280, Proceedings of the 19th International Technical Conference on the Enhanced Safety of Vehicles (ESV), Washington DC, United States.

[22] Youn Y., Kim S., Oh C., Shin M., Lee C. (2005) Research and Rule-Making Activities on Pedestrian Protection in Korea, Paper 05-0117, Proceedings of the 19th International Technical Conference on the Enhanced Safety of Vehicles (ESV), Washington DC, United States.

[23] World Bank Group: Road Safety, (2007). <http://www.worldbank.org/html/fpd/transport/roads/safety.htm> (accessed February 6 2007).

APPENDIX

Scaling of Rigid Parts

A rigid part is usually defined in a FE model by its mass m and the components of the mass moment of inertia tensor I with respect to a local coordinate system with the origin at the rigid body center of gravity (CG). To find a relationship between the inertial properties of a rigid body obtained by scaling and its initial inertial properties (in original configuration) the following theorem will be used.

Theorem

Assume a rigid body with the mass m and the mass moment of inertia tensor I with respect to a local coordinate system $oxyz$ (the direction of the local axes parallel to the global axes), and $o(x,y,z)$ – the center of gravity (Figure A1).

(A.1)

Assume a linear transformation (scaling) with respect to the global coordinate system $O_1x_1y_1z_1$ with scale factors $\lambda_x, \lambda_y, \lambda_z$ and a constant mass density between models. Thus, the mass of the scaled model will be:

$$M = m\lambda_x\lambda_y\lambda_z \quad (A.2)$$

and the components of the inertia tensor with respect to the new local coordinate system $O(\lambda_x x_o, \lambda_y y_o, \lambda_z z_o)$ will be:

$$I_{xx} = \lambda_x\lambda_y\lambda_z(\lambda_y^2 J_y + \lambda_z^2 J_z) \quad (A.3)$$

$$I_{yy} = \lambda_x\lambda_y\lambda_z(\lambda_x^2 J_x + \lambda_z^2 J_z)$$

$$I_{zz} = \lambda_x\lambda_y\lambda_z(\lambda_x^2 J_x + \lambda_y^2 J_y)$$

(A.4)

where

$$I_{xy} = \lambda_x^2\lambda_y^2\lambda_z I_{xy}$$

$$I_{xz} = \lambda_x^2\lambda_y\lambda_z^2 I_{xz}$$

$$J_x = (I_{yy} + I_{zz} - I_{xx})/2$$

$$J_y = (I_{zz} + I_{xx} - I_{yy})/2 \quad (A.5)$$

$$J_z = (I_{yy} + I_{xx} - I_{zz})/2$$

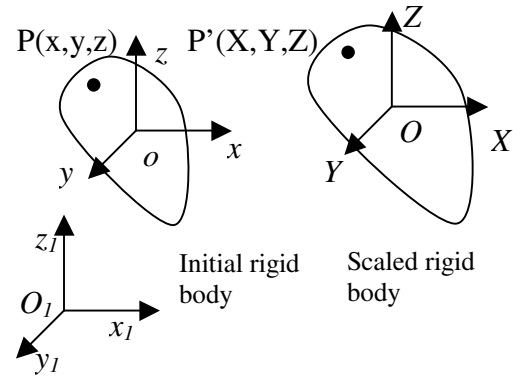


Figure A1: Rigid body in initial and scaled configurations; A particular case - the axes of local system are parallel to those of the global system.

Proof

Linear scaling (transformation) with respect to the global system $O_1x_1y_1z_1$ will move each point P of the original body (Ω) which has a coordinate (x,y,z) with respect to the system $oxyz$ and coordinate (x_1,y_1,z_1) with respect to the system $O_1x_1y_1z_1$ into the point P' of scaled body (Ω') which has coordinate (X,Y,Z) with respect to the system $OXYZ$ and coordinate (X_1,Y_1,Z_1) with respect to the system $O_1x_1y_1z_1$ (Figure A1).

$$X_1 = \lambda_x x_1 = \lambda_x x + \lambda_x x_{o1} = \lambda_x x + x_o$$

$$\text{Thus, } X = \lambda_x x$$

Similarly it can be shown that

$$Y = \lambda_y y \quad Z = \lambda_z z$$

Thus, the scaled diagonal components of inertia tensor will be:

$$I_{xx} = \int_{\Omega'} (Y^2 + Z^2) \rho dV = \int_{\Omega} (\lambda_y^2 y^2 + \lambda_z^2 z^2) \rho \lambda_x \lambda_y \lambda_z dv$$

$$= \lambda_x \lambda_y \lambda_z (\lambda_y^2 J_y + \lambda_z^2 J_z)$$

Similar it can be shown that

$$I_{yy} = \lambda_x \lambda_y \lambda_z (\lambda_x^2 J_x + \lambda_z^2 J_z)$$

$$I_{zz} = \lambda_x \lambda_y \lambda_z (\lambda_x^2 J_x + \lambda_y^2 J_y)$$

The scaled off-diagonal components of inertia tensor will be

$$I_{xy} = \int_{\Omega'} YZ \rho dV = \int_{\Omega} \lambda_x \lambda_y xy \rho \lambda_x \lambda_y \lambda_z dv$$

$$= \lambda_x^2 \lambda_y^2 \lambda_z J_{xy}$$

Similarly it can be shown that

When the axes of the local coordinate system are not parallel to corresponding axes of the global system (Figure A2), the components of mass inertia tensor in the new local system of a scaled rigid body OXYZ can be determined by according to the following procedure:

1. Obtain the inertia tensor i' with respect to a system $ox'y'z'$ with axes parallel to the global coordinate system $O_1x_1y_1z_1$ from the mass inertia tensor i from the initial coordinate system $oxyz$.

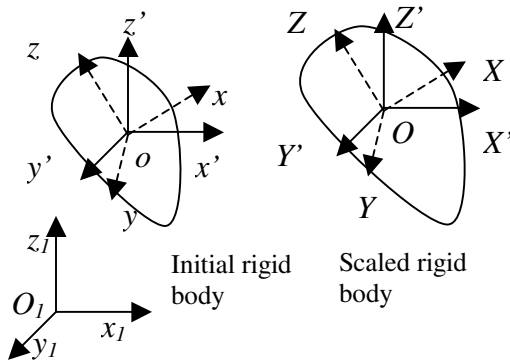


Figure A2: Rigid body in initial and scaled configurations; general case

The inertia tensor i' will be:

$$i' = Q i Q^T \quad (A.6)$$

where Q is the transformation matrix (orthogonal matrix) between $oxyz$ and $ox'y'z'$.

2. Obtain the inertia tensor I' of the scaled rigid body with respect to a system $OX'Y'Z'$ (with the axes parallel to the global system axes) using [A.3 – A.4] equations.
3. Obtain the inertia tensor I with respect to a system $OXYZ$ with axes parallel to the initial local coordinate system $oxyz$

Thus, the inertia tensor I will be:

$$I = Q^T I' Q \quad (A.7)$$